

Design of a Coplanar UWB-MIMO Ground Antenna Based on the Theory of Characteristic Modes

Zhijun Tang^{1, 2, 3, *}, Jie Zhan^{1, 2}, Bin Zhong¹, Long Chen¹, and Guocai Zuo³

Abstract—A novel two-element UWB-MIMO ground antenna is designed by using the theory of characteristic modes. The proposed antenna has a simple and compact coplanar structure, which consists of a rectangular metal ground, a four-stage stepped patch, a double L-shaped patch with a corner cut, and a rectangular substrate. By analyzing the most relevant characteristic modes of the metal ground in UWB, the expected characteristic modes are excited by the capacitive coupling elements and the hybrid loading of the capacitive and inductive coupling elements, so as to reduce the size, broaden the bandwidth, and improve the isolation. The simulated and measured results show that the proposed antenna obtains ultra-wide impedance bandwidths (2.7–12.6 GHz for Port 1 and 3.0–11.0 GHz for Port 2). Furthermore, the proposed antenna also achieves high gains (3.1–7.3 dBi for Port 1 and 2.7–5.8 dBi for Port 2), stable radiation patterns, and good diversity characteristics (the minimum isolation > 16 dB, the envelope correlation coefficient < 0.01 , the channel capacity loss < 0.08 bps/Hz, the total active reflection coefficient < -4.1 dB, etc.) in the whole impedance bandwidth. The research results can provide a useful reference for the design of UWB-MIMO ground antennas based on the theory of characteristic modes.

1. INTRODUCTION

With the rapid development of communication technology, large channel capacity and high frequency spectral efficiency have become the urgent needs of the next generation mobile access technology. In order to realize the development of wireless communication in the direction of large capacity, wide bandwidth, and high-frequency spectrum utilization, it is necessary to break through the bottleneck of traditional communication in these aspects. In recent years, ultra-wideband (UWB) technology based on ultrashort pulse has increasingly shown its unique advantages and attracted extensive attention because of its advantages such as high data rate, accurate positioning, low power spectral density, low power consumption, low complexity and cost [1–3]. However, UWB technology also has several shortcomings. Its upper limit radiated power spectral density is -41.3 dBm/MHz, which will cause UWB system to be interfered by other narrowband wireless communications, resulting in low signal-to-noise ratio, poor signal reliability, and bad communication quality. At the same time, when the power of a UWB system is limited, the UWB system can only realize short-distance high-speed transmission, which is difficult to realize long-distance transmission. In addition, a UWB channel belongs to the high frequency selective fading channel, which is easy to produce very serious inter symbol crosstalk. The recently emerging multi-input multi-output (MIMO) technology can effectively decompose a communication link into multiple parallel sub communication channels, turn the multipath fading that is not conducive to wireless communication into a favorable factor, and improve the reliability of system data transmission. On the

Received 12 November 2021, Accepted 22 December 2021, Scheduled 6 January 2022

* Corresponding author: Zhijun Tang (zjtang@hnust.edu.cn).

¹ School of Information and Electrical Engineering, Hunan University of Science and Technology, Xiangtan 411201, China. ² Science and Technology on Communication Networks Laboratory, Shijiazhuang 050081, China. ³ Hunan Software Vocational and Technical University, Xiangtan 411100, China.

other hand, MIMO technology can multiply the channel capacity and improve the spectrum efficiency by using spatial multiplexing. Therefore, researchers suggest that UWB technology and MIMO technology are organically combined into UWB-MIMO technology [4, 5], which can solve the shortcomings of UWB technology and cater to the requirements of green communication concept rising all over the world in recent years and future wireless access technology. As an indispensable device for the realization of this technology, UWB-MIMO antenna is receiving extensive attention from scholars [6–9].

At present, the research on UWB-MIMO antennas mainly focuses on miniaturization, bandwidth broadening, improving isolation, generating notches [10–14], etc. Among them, while considering the application requirements of antenna geometry, broadening antenna bandwidth and improving the isolation between antenna units are the top priorities in UWB-MIMO antenna design. At present, bandwidth broadening methods mainly use multi-type monopole antennas [15–17], slot antennas [18], gradient structure antennas [19], fractal antennas [20], meander technology [21], etc. On the other hand, the methods or technologies to improve the isolation mainly include increasing resonant structure, decoupling network [22], neutral line [23], orthogonal geometric arrangement [24, 25], defective ground structure (DGS) [26] with the extended ground stubs [25], electromagnetic band gap (EBG) [27], mode diversity [28], metamaterials and metasurfaces [29, 30]. The existing UWB-MIMO antennas are usually designed with multi-layer plane or three-dimensional structure. Although coplanar waveguide (CPW) UWB-MIMO antenna is a single-layer metal structure, its radiator and ground plane are independent and separated, and the ground plane is not the main radiator. However, the compact application scenarios of modern wireless mobile terminals or platforms require their antennas to have miniaturized, low profile, conformal and other geometric structures. In such applications, the metal ground is the main radiator, the radiation patch structure should be simple, and its function is to excite the metal ground radiation efficiently. In particular, the housing or chassis of the mobile terminal acts not only as a radiator, but also as a ground plane [31]. However, the current MIMO antennas with single-layer shared structure have limited application fields due to its narrow bandwidth, low isolation, and large size. Therefore, in order to solve the problems of the above single-layer shared structure ground antennas, it is necessary to develop the UWB-MIMO antenna design principle or method into the ground antenna. In recent years, there are more and more reports on the application of theory of characteristic mode (TCM) in UWB antenna or MIMO antenna design, mainly focusing on impedance optimization, bandwidth broadening, and reducing correlation [32–34]. However, there are relatively few reports on the research and application of TCM in UWB-MIMO antenna [35], especially coplanar UWB-MIMO antennas [36]. Most of the reported UWB-MIMO antennas designed based on TCM do not fully cover the frequency band range (3.1–10.6 GHz) specified by the Federal Communications Commission (FCC).

In this paper, a coplanar two elements UWB-MIMO ground antenna structure is proposed. Firstly, based on the characteristic mode theory, the most relevant characteristic modes and characteristic current distributions of a rectangular metal ground in UWB band are analyzed in order to determine the feeding position and method of antenna unit 1, and a four-stage stepped radiation patch is introduced to excite the desired characteristic modes by a capacitive loading. Then, using the same mechanism and method, the feeding position and way of antenna unit 2 are determined. The metal ground with a notch and the double L-shaped patch with a chamfer are introduced, and the expected characteristic modes are excited by a capacitive and inductive mixed loading. Finally, multiple characteristic modes and linear combinations of multiple characteristic modes are excited at different ports of the antenna, so as to broaden the impedance bandwidth and improve the isolation.

2. DESIGN METHOD OF UWB-MIMO ANTENNA BASED ON TCM

Characteristic mode theory combines the advantages of analytical method and numerical method. It can not only give a clear physical explanation to the solution results, but also be used to solve the electromagnetic field problems of objects with arbitrary shapes. Because the radiation characteristics of an antenna are determined by the current distribution on its surface, analyzing the current distribution on the antenna surface based on TCM can study the main factors affecting the antenna performance from the physical essence, and can provide valuable information for antenna design. The analysis of radiation and scattering characteristics of arbitrary geometric structures based on characteristic mode theory usually starts from solving the eigenvalue problem, and the solution of any electromagnetic field

problem can be expressed as a linear combination of eigenmodes. These characteristic modes have orthogonality and convergence, and express the inherent electromagnetic characteristics of the object. The eigenvalue numerical calculation can be carried out by solving the eigenvalue equation in the matrix form of Equation (1) [37].

$$[X(\omega)][\vec{J}_n(\omega)] = \lambda_n(\omega)[R(\omega)][\vec{J}_n(\omega)] \tag{1}$$

where $[R(\omega)]$ and $[X(\omega)]$ are the real and imaginary parts of impedance matrix $[Z(\omega)]$ respectively; $\lambda_n(\omega)$ is the eigenvalue; $[\vec{J}_n(\omega)]$ is the characteristic current. It should be noted that it is very challenging to calculate the eigenvalues of all modes in UWB. In addition to the eigenvalues, the characteristic mode parameters also include characteristic angle (CA) and mode significance (MS), which can be calculated by Equations (2) and (3), respectively:

$$\theta_n = 180^\circ - \tan^{-1} \lambda_n \tag{2}$$

$$MS = \left| \frac{1}{1 + j\lambda_n} \right| \tag{3}$$

It should be noted that the three parameters of eigenvalue, characteristic angle and mode significance are equivalent, and one of them can be used in characteristic mode analysis (CMA). When the eigenvalue of a mode is equal to 0, the mode produces resonance. The smaller the eigenvalue is, the easier the mode is excited at this frequency point. When the characteristic angle of a mode is equal to 180° , the mode resonates. In other words, the closer the characteristic angle is to 180° , the more likely it is to produce resonance. If the CA of a mode is close to 180° in a certain frequency band, it indicates that the mode may produce resonance in the whole frequency band and has a broadband potential. When the mode significance of a mode is close to 1, the mode is more likely to produce resonance. For the sake of intuition, the characteristic angle and mode significance parameters are usually selected in the characteristic mode analysis. Isolation and envelope correlation coefficient are important parameters to measure the mutual coupling between MIMO antenna elements. In order to use characteristic mode theory analysis to guide MIMO antenna design, it is necessary to analyze the description of these two parameters in characteristic mode theory. Using the orthogonality of the characteristic current, the total current is expanded according to the mode of the characteristic current, and the mutual admittance from the excitation port to other ports can be deduced [38], as shown in formula (4).

$$Y_{ji} = \sum_n a_n J_n(j) l_e = \sum_n l_e^2 \frac{J_n(i)}{1 + j\lambda_n} J_n(j) \tag{4}$$

where a_n is the weighting coefficient of the n th mode, and l_e is the length of the common edge of the basis function at the feed port. As can be seen from Equation (4), when each port of the antenna matches well (the impedance is near 50 Ohm), the smaller the current is generated by the coupling of the excitation port at other ports, the smaller its mutual admittance is, and the higher the isolation of the antenna is. Then, using the orthogonality of the characteristic electric field, expand the total electric field generated by the excitation port and other ports according to the characteristic electric field, and the envelope correlation coefficient can be deduced, shown in formula (5):

$$\rho_{ji} = \left| \sum_{n=1}^N a_{n,i} \cdot a_{n,j}^* \right|^2 / \left(\left(\sum_{n=1}^N |a_{n,i}|^2 \right) \cdot \left(\sum_{n=1}^N |a_{n,j}|^2 \right) \right) \tag{5}$$

Equation (5) shows that the correlation coefficient between antenna elements can excite a specific characteristic mode among all ports by adjusting the port excitation position, amplitude, and phase of these ports, so as to realize the orthogonal characteristic.

The characteristic mode theory is used to guide MIMO antenna design. Ideally, different antenna units are expected to work in different modes, and these modes are orthogonal to each other, so as to improve the isolation between antenna units. However, if this single different characteristic mode orthogonal method is adopted, it usually needs to design a complex antenna structure or feed network, and the bandwidth broadening degree of the antenna is limited. Therefore, in order to reduce the complexity of an antenna or a feed network design and to broaden the bandwidth, based on the physical mechanism of Equations (4) and (5), the linear combination of multiple characteristic modes can be

adopted to realize the low isolation characteristic: different ports realize the linear combination of different characteristic modes; different ports realize the linear combination of the same characteristic mode; the first two cases are mixed.

Based on the characteristic mode theory, the antenna can be fed by capacitive and inductive methods. The excitation of inductive coupling element (ICE) is usually realized by cutting directly on the radiator, and ICE is a direct inductive excitation [39]. The excitation of capacitive coupling element (CCE) is achieved by adding a metal patch near the edge of the radiator, and ICE is a direct capacitive excitation [40]. In general, the corresponding mode can be resonated by ICE at the position of the maximum current distribution of the characteristic mode [41–43]. On the other hand, applying CCE at the position where the characteristic mode current distribution is the minimum can also make the corresponding mode resonate [44, 45]. It should be pointed out that ICE is usually easier to excite a pure single characteristic mode than CCE for narrowband antennas. However, for UWB antenna design, it is usually necessary to excite multiple characteristic modes in order to broaden the bandwidth. Therefore, CCE or the hybrid excitation of CCE and ICE are usually used for UWB antenna design.

After loading the excitation source, the contribution of each characteristic mode to the overall radiation of the antenna can be determined by calculating the mode weighting coefficient (MWC), which plays a guiding role in the adjustment of the antenna structure. When the antenna has multiple ports, the feed position of other ports can also be determined by the mode weighting coefficient, which plays an important guiding role in dealing with the isolation between ports. The MWC can be calculated by Equation (6).

$$\text{MWC} = \frac{[V]^T [J]_n}{1 + j\lambda_n} \quad (6)$$

where $[V]$ is the excitation source vector.

It should be emphasized that compared with MIMO antenna, UWB-MIMO antenna design guided by characteristic mode analysis should consider not only isolation requirements, but also bandwidth requirements. Therefore, for UWB-MIMO antennas, in order to broaden the antenna bandwidth, it is usually necessary to excite multiple characteristic modes in the UWB frequency band. Compared with narrowband MIMO antenna, the broadband, especially UWB-MIMO antenna mode excitation is more challenging.

3. ANTENNA DESIGN AND CHARACTERISTIC MODE ANALYSIS

As shown in Fig. 1(a), we analyzed the characteristic modes of a rectangular metal ground with a size of $50 \text{ mm} \times 40 \text{ mm}$ in UWB and determined the way to excite the corresponding characteristic mode by observing the change of its characteristic mode and corresponding surface current with frequencies. Electromagnetic simulation software CST 2019 and FEKO 2019 are used for antenna design and simulation analysis.

The characteristic angle and mode significance of the first five most relevant characteristic modes of the rectangular metal ground in the UWB band are shown in Fig. 2. As can be seen from Fig. 2(a), the first five most relevant characteristic modes resonate at frequencies of 2.9 GHz, 4.3 GHz, 5.0 GHz,

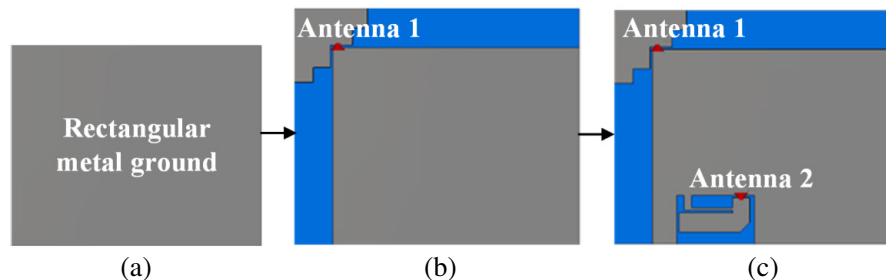


Figure 1. The design process of a radiator-ground shared antenna: (a) rectangular patch, (b) loading a stepped patch, (c) loading a double L-shaped patch.

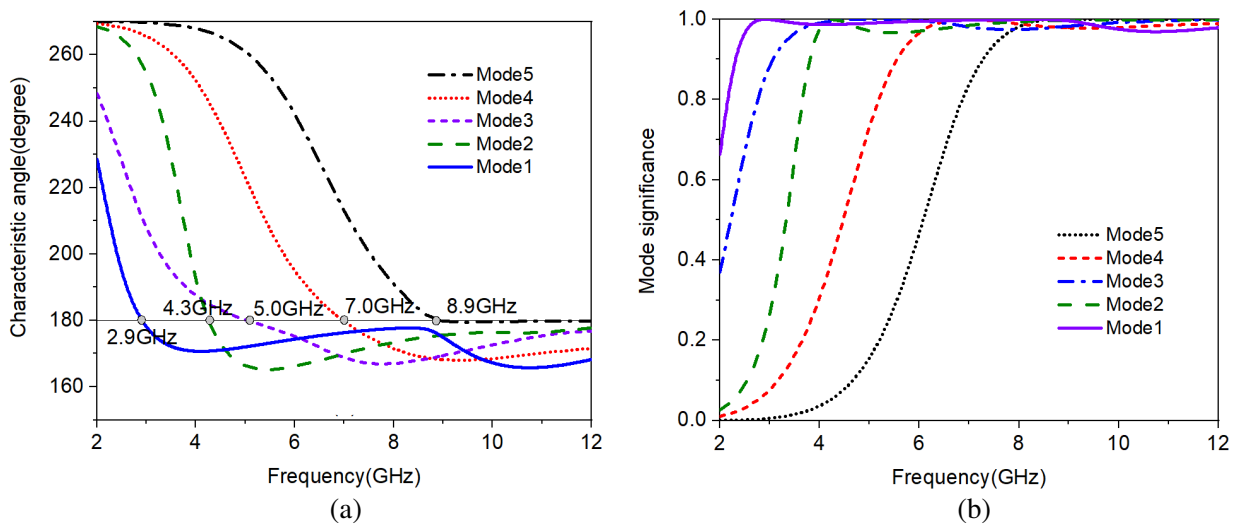


Figure 2. Prediction of the first five most relevant characteristic modes of the rectangular metal ground in UWB, (a) characteristic angle, (b) mode significance.

7.0 GHz, and 8.9 GHz, respectively. Among them, the characteristic angle of mode 1 is close to 180° in the whole UWB, indicating that the mode has good resonance characteristics in the whole UWB. The other four modes also have good resonance characteristics from their resonance point to UWB high frequency band. The mode significance shown in Fig. 2(b) further confirms the resonant characteristics of the five most relevant characteristic modes of the rectangular metal ground in UWB. Therefore, in order to realize the UWB characteristics of the antenna, these resonant modes should be excited as much as possible.

As mentioned above, in order to satisfy the UWB broadband requirements of the antenna, the loaded antenna should excite as many resonant modes of the metal ground in the UWB as possible. The loading method of the antenna mainly determines whether to feed the antenna in capacitive or inductive mode by observing and analyzing the surface current distribution of the characteristic mode. In view of this, the surface current distributions of the first five most relevant modes of the rectangular metal ground at its corresponding resonance point are shown in Fig. 3. As can be seen from Fig. 3, the strongest surface current distribution in mode 1 is in the middle of the long side, while mode 2, mode 3, mode 4, and mode 5 are in the middle of the long and short sides, the middle of the short side, both sides of the middle of the long side, and the center, respectively. Therefore, it is difficult to excite more resonant modes by ICE excitation, which is not conducive to broadening the antenna bandwidth. On the other hand, it is observed that these five modes have the weakest or weaker surface current distribution at the metal ground corner. Therefore, loading CCE excitation near the metal ground corner can excite more resonant modes of the metal ground, so as to broaden the antenna bandwidth.

According to the existing literature reports, circular, square, and stepped patches have broadband potential. However, considering the miniaturization of the antenna and the actual physical structure of the metal ground, a four-stage stepped metal patch is introduced near the diagonal of the metal ground to load antenna 1 by the CCE, as shown in Fig. 1(b). It should be pointed out that considering the symmetry of antenna geometry and loading position, only even-stage stepped patches are selected. Although the two-stage structure is simple, some performances are difficult to meet the requirements. The six or more stage structure will increase the geometric size of the antenna, and its main performance is not better than the four stage structure. As described in Section 2, in order to verify whether the CCE loading can successfully excite multiple resonant modes of the metal ground and the overall radiation contribution of these modes to the antenna, it is necessary to calculate the mode weighting coefficient of the antenna after loading excitation.

The mode weighting coefficient of the metal ground after loading antenna 1 is shown in Fig. 4. It can be observed that in the low frequency band, mode 1 has a large weight, and mode 2 has a maximum

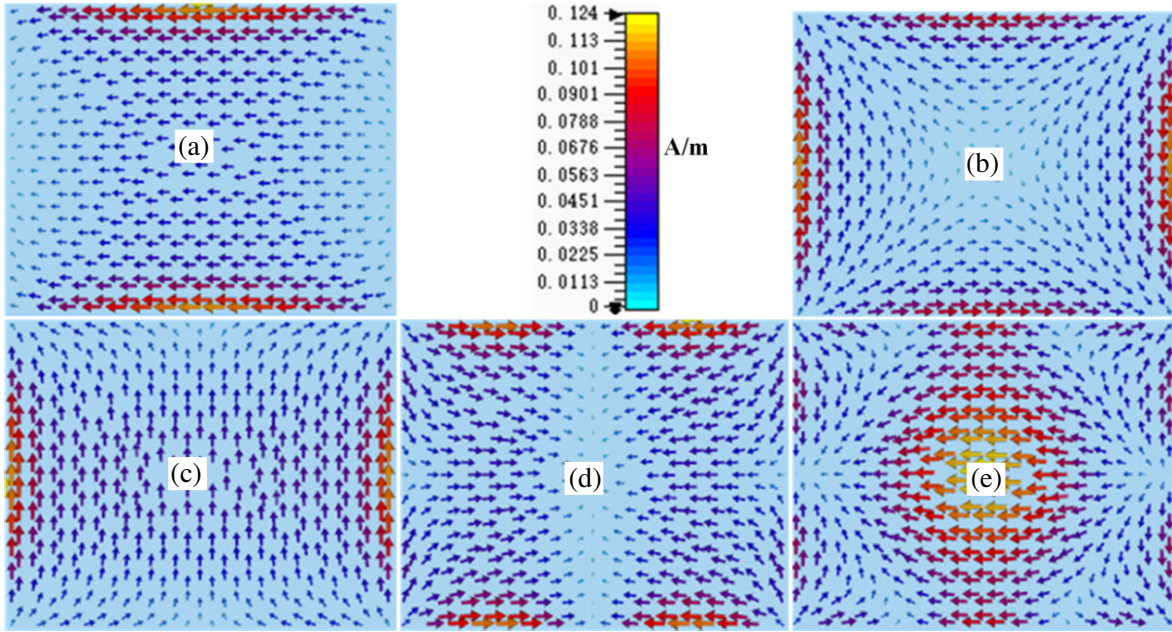


Figure 3. Surface current distribution of the rectangular metal ground, (a) mode 1 at 2.9 GHz, (b) mode 2 at 4.3 GHz, (c) mode 3 at 5.0 GHz, (d) mode 4 at 7.0 GHz, (e) mode 5 at 8.9 GHz.

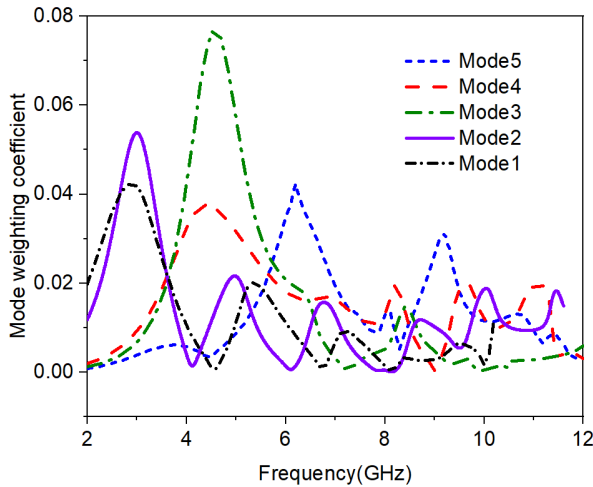


Figure 4. Mode weighting coefficient of the metal ground after loading antenna 1.

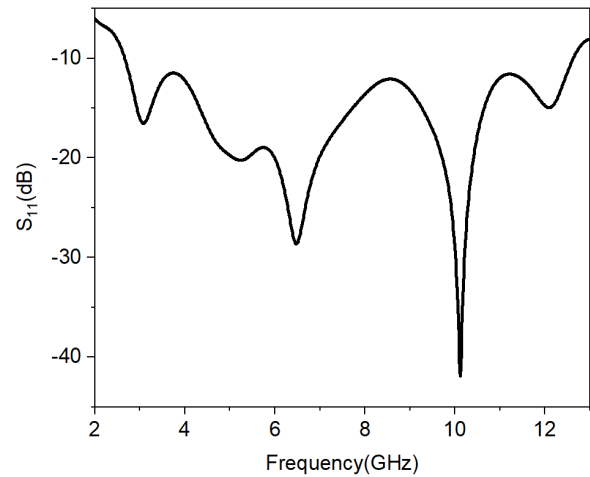


Figure 5. Reflection characteristics of antenna 1 when antenna 2 is not loaded.

weight. In the lower and intermediate frequency bands, mode 3 has the largest weight, and mode 4 and mode 5 have a larger weight. In the high frequency band, mode 5 has the largest weight, and mode 4 and mode 1 also have large weight. Therefore, after loading the four-stage stepped patch, multiple resonant modes of the metal ground in UWB are successfully excited. The reflection coefficient (S_{11}) of antenna 1 after adding the substrate is shown in Fig. 5. It can be seen that the antenna generates resonance at about 3.0 GHz, 5.0 GHz, 6.5 GHz, 10.0 GHz, and 12.0 GHz, which is in good agreement with the above characteristic mode analysis results. The bandwidth of antenna 1 is 9.9 GHz (2.7–12.6 GHz), which fully covers the UWB (3.1–10.6 GHz) specified by FCC.

In order to achieve the purpose of designing a MIMO antenna, after successfully loading the antenna 1, another excitation needs to be added to complete the design of antenna 2. According

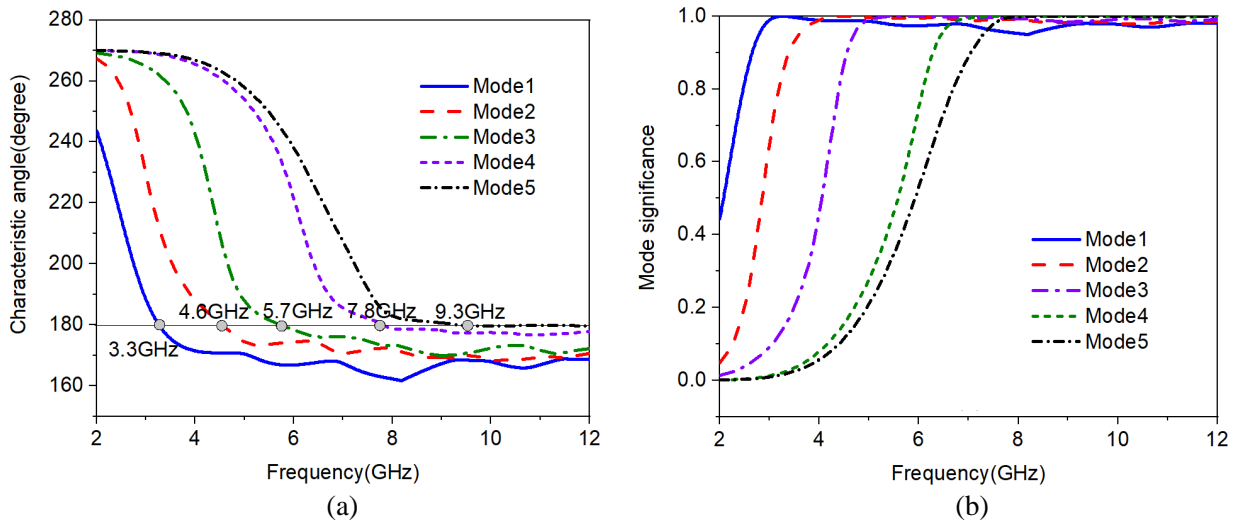


Figure 6. Prediction of the first five most relevant characteristic modes of the metal ground in UWB after loading antenna 1, (a) characteristic angle, (b) mode significance.

to the above design principles and methods, in order to determine the position and way of excitation loading, it is necessary to reanalyze the characteristic mode of the metal ground after loading antenna 1. The prediction of the first five most relevant characteristic modes of the metal ground in UWB is shown in Fig. 6. It can be seen that these modes produce resonances at 3.3 GHz, 4.6 GHz, 5.7 GHz, 7.8 GHz, and 9.3 GHz, respectively. Moreover, in the UWB, the characteristic angle and mode significance of these modes are close to 180° and 1, respectively, indicating that they have UWB potential. How to excite these modes requires the further observation of the current distribution of these characteristic modes.

Figure 7 shows the characteristic mode current distribution of the metal ground after loading port 1. It can be observed that mode 2 and mode 4 have the weakest current distribution at the lower left of the metal ground. Mode 1 and mode 3 have stronger current distribution at the lower left of the metal ground, while the characteristic currents of mode 5 have alternating strong and weak distribution in this area. Therefore, in order to excite multiple mode resonances of the metal ground and make antenna 2 also obtain UWB characteristics, it is necessary to introduce a suitable loading patch structure. In order to achieve the above purpose, a rectangular slit is introduced at the appropriate position at the lower left of the metal ground, and a double L-shaped patch with a chamfer and a hybrid excitation of CCE and ICE are introduced to design antenna 2, as shown in Fig. 1(c).

The mode weighting coefficient of the metal ground is shown in Fig. 8 after antenna 2 is loaded. It can be observed that mode 1, mode 2, and mode 3 have large weight in UWB low frequency band. In UWB medium frequency band, mode 3, mode 1, and mode 4 have large weight. In UWB high frequency band, mode 5 and mode 4 have large weight. These show that the double L-shaped patch can successfully excite multiple resonant modes of the metal ground in UWB.

The reflection coefficient (S_{22}) of antenna 2 is shown in Fig. 9 after adding the substrate. It can be observed that antenna 2 generates resonances at about 3.3 GHz, 5.0 GHz, 6.1 GHz, 7.7 GHz, and 10.0 GHz, which are in good agreement with the above characteristic mode analysis results of the metal ground after antenna 1 is loaded. Antenna 2 achieves a bandwidth of 8.0 GHz (3.0–11.0 GHz). In addition, by comparing the reflection coefficient characteristics of antenna 1 before and after loading antenna 2, it can be seen that the bandwidth of antenna 1 remains basically unchanged, and the resonance characteristics of antenna 1 are further enhanced after loading antenna 2. The impedance bandwidths of antenna 1 and antenna 2 completely cover the ultra-wideband specified by FCC.

4. RESULTS AND DISCUSSIONS

4.1. Geometric Structure and Parameters

The geometric structure and parameters of the UWB-MIMO ground antenna are shown in Fig. 10. The antenna is printed on a Rogers RO3003 substrate. The thickness of the substrate is 1.6 mm; the relative dielectric constant is 3.0; and the loss tangent is 0.001. The antenna has a simple and compact single-layer metal structure, and antenna 1 (port 1) is formed by introducing a four-stage stepped patch at the opposite corner of a rectangular metal ground. Antenna 2 (port 2) is designed by cutting a small rectangle at the lower left of the opposite side of antenna 1 and introducing a double L-shaped patch with a chamfer. Both port 1 and port 2 are connected by RF cables. The geometric parameters and optimized dimensions of the designed antenna are shown in Table 1. The prototype and test scenario of the antenna are shown in Fig. 11.

Table 1. The geometric parameters and optimized dimensions of the antenna (unit: mm).

Parm	Dimension	Parm	Dimension	Parm	Dimension	Parm	Dimension
L_s	58	W_s	48	L_1	50	W_1	40
L_2	16	W_2	10	L_p	15	t_1	3
t_2	4	$a1$	7.1	$a2$	12.5	$a3$	2
$S1$	3.5	$S2$	4	$S3$	0.5	$S4$	1.5

4.2. Bandwidth and Isolation Characteristics

The reflection coefficient (S_{11} or S_{22}) of S -parameters is an important parameter to characterize the antenna bandwidth, and the transmission coefficient (S_{12} or S_{21}) is an important parameter to

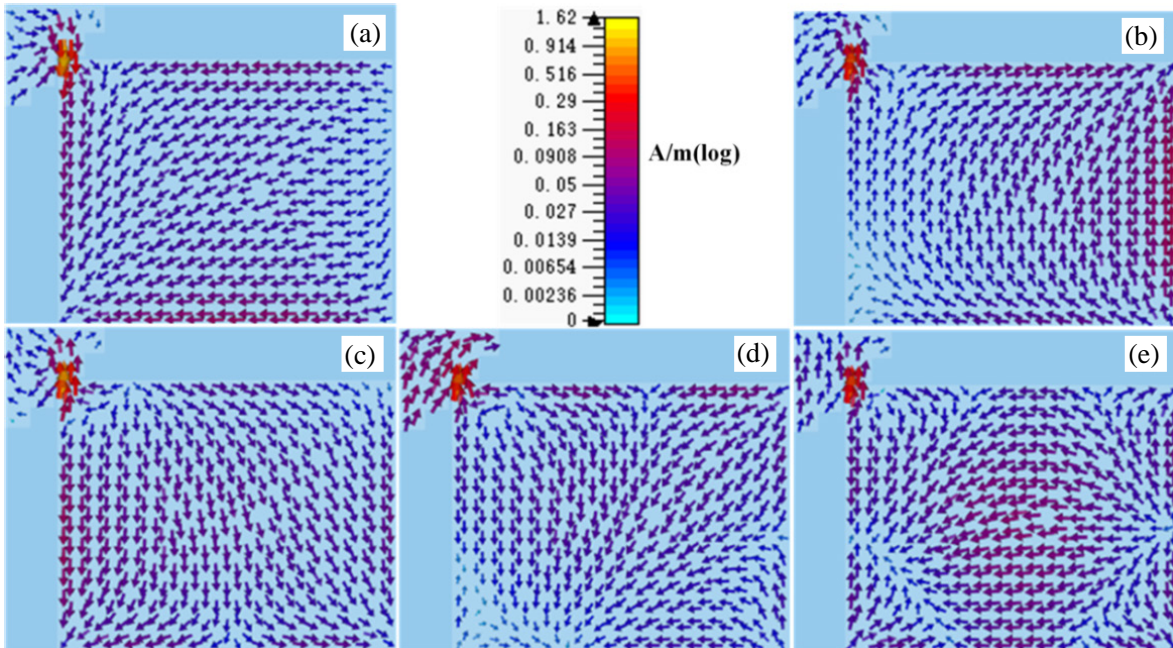


Figure 7. Characteristic mode current distribution of the metal ground after loading port 1: (a) mode 1 is at 3.3 GHz, (b) mode 2 at 4.6 GHz, (c) mode 3 at 5.7 GHz, (d) mode 4 at 7.8 GHz, (e) mode 5 is at 9.3 GHz.

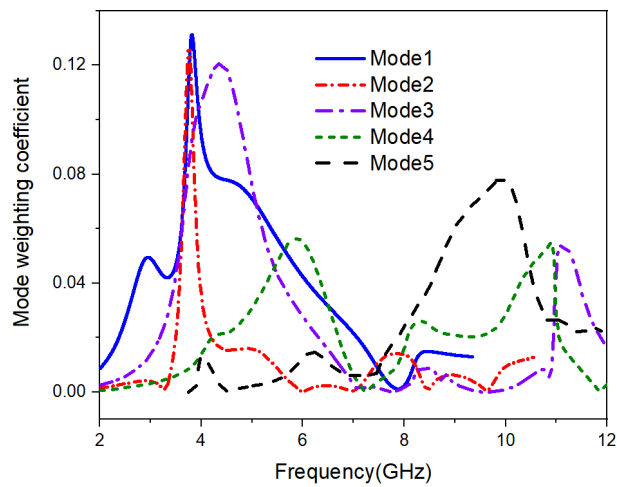


Figure 8. Mode weighting coefficient of the metal ground after antenna 2 is loaded.

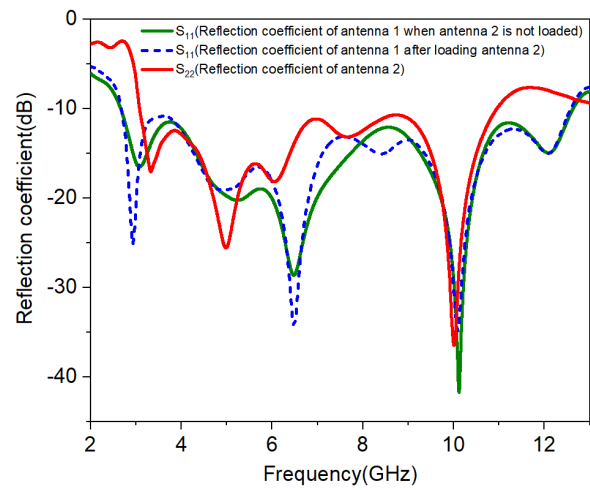


Figure 9. Reflection characteristics of the proposed UWB-MIMO antenna.

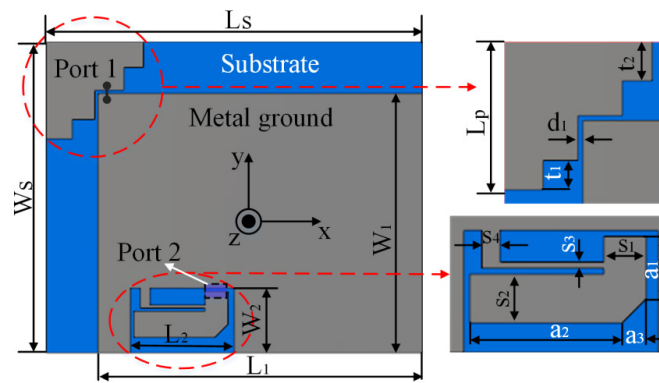


Figure 10. Geometric structure and parameters of the designed antenna.

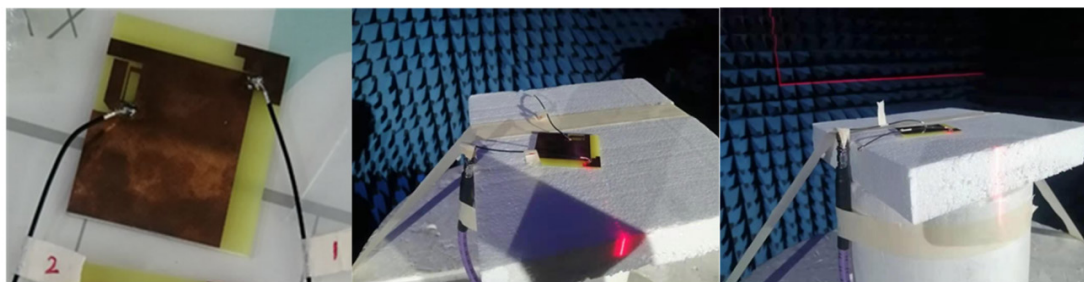


Figure 11. The prototype and test scenario of the proposed antenna.

characterize the isolation between multiple antenna units ($|S_{21}|$ or $|S_{12}|$). Fig. 12 shows the variation of S -parameters of the designed antenna with frequency. Antenna 1 can obtain 9.9 GHz (2.7–12.6 GHz) bandwidth or a fractional bandwidth of 129.4%. Antenna 2 can finally obtain 8.0 GHz (3.0–11.0 GHz) bandwidth or a fractional bandwidth of 114.3%. The transmission coefficient S_{21} is large only in the narrow band (3.2–4.3 GHz) of the impedance bandwidth, but it is also less than -16 dB, and less than

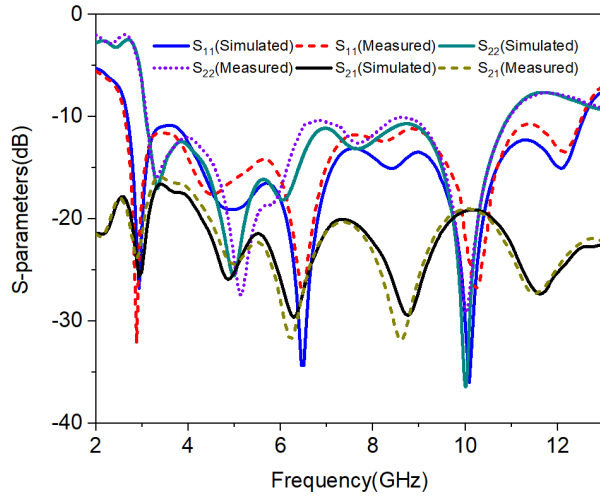


Figure 12. S -parameters of the proposed antenna.

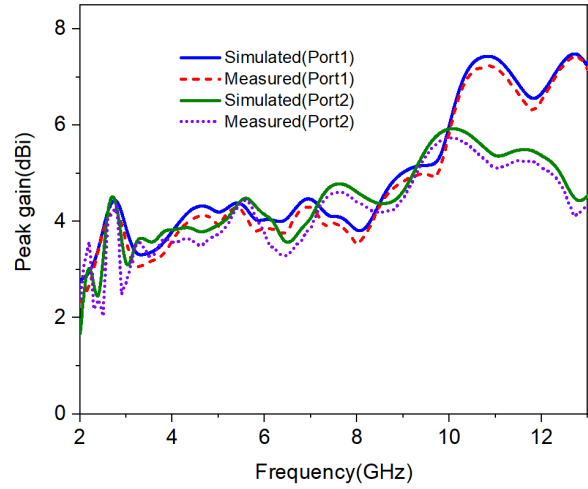


Figure 13. Peak realized gains of the proposed antenna.

-20 dB in other frequency bands of the impedance bandwidth. Therefore, the bandwidth of the designed UWB-MIMO ground antenna fully covers the UWB frequency, and its minimum isolation $|S_{21}|$ is greater than 16.0 dB. Furthermore, its isolation is greater than 20.0 dB in nearly 90% of the bandwidth.

4.3. Gain and Radiation Characteristics

The peak gains of the designed antenna are measured in three-dimensional domain by using a comparison method. When the peak gains of a single port is measured, the other port is in a matching state. In the process of the measurement, the standard antenna (horn antenna) needs to be placed in the quiet area of the anechoic chamber together with the antenna support and feeding device. In general, the non-uniformity of the support, feeding device, and static area field in the environment of the anechoic chamber interfere with the measurement results of the received power of the standard antenna, and

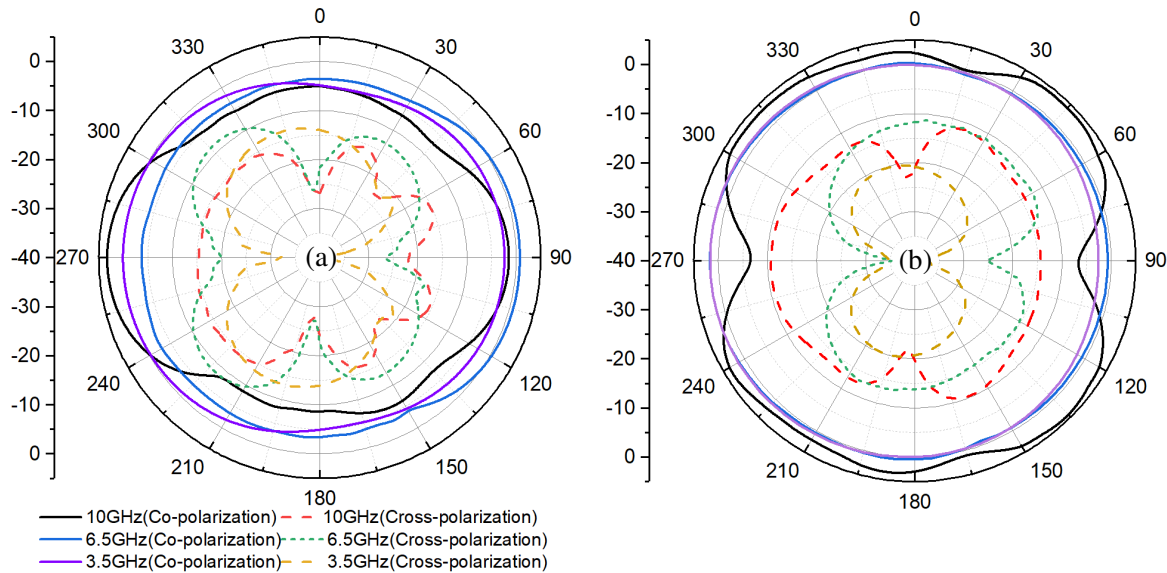


Figure 14. Radiation patterns of the proposed antenna in the E -plane, (a) port 1, (b) port 2.

then affect the measuring accuracy of the peak gains. Therefore, the influence of the above factors should be minimized in the process of the peak gain measurements. The variation of the peak realized gain of the antenna with frequency is shown in Fig. 13. It can be observed that the peak realized gain of antenna 1 varies from 3.1 to 7.3 dBi within its impedance bandwidth. The gain of low and intermediate frequency band is stable at about 3.1–5.0 dBi, while the gain of high frequency band is increased from 5.0 to 7.3 dBi, which is mainly due to the partial orientation of excitation and radiation modes of high-order modes at higher frequencies. In the whole impedance bandwidth, the variation range of the peak realized gain of antenna 2 is 2.7–5.8 dBi. The small fluctuation of the peak gain in some frequency bands is mainly caused by the non-resonant characteristics of the antenna. Considering the UWB characteristics of the antenna, the designed UWB-MIMO ground antenna has stable gains.

The coplanar polarization and cross polarization performance measurements of *E*-plane and *H*-plane at 3.5 GHz, 6.5 GHz, and 10 GHz are shown in Fig. 14 and Fig. 15, respectively. It can be observed that the antenna has stable radiation characteristics in the whole UWB. The further observation shows that the radiation patterns in the low frequency band are better than those in the high frequency band, and have quasi-omnidirectional characteristics. The high frequency band mainly excites the high-order modes of the metal ground. Therefore, the omnidirectivity of its radiation is not as good as that of the low-frequency band. In general, considering the trade-off requirements of the main performance parameters of the designed antenna, it has relatively stable radiation characteristics in the whole UWB.

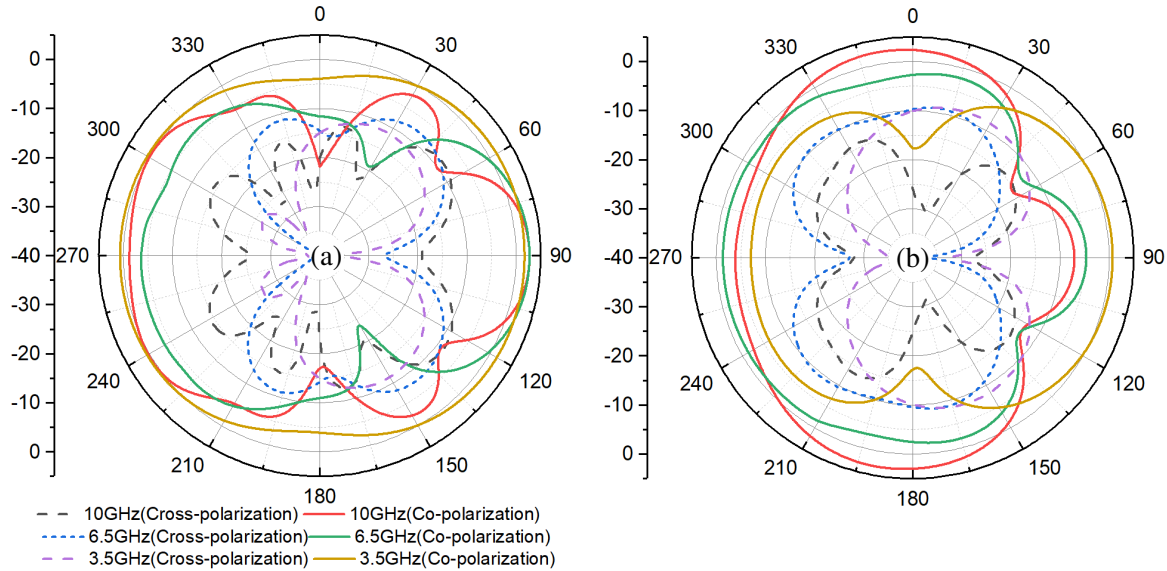


Figure 15. Radiation patterns of the proposed antenna in the *H*-plane, (a) port 1, (b) port 2.

4.4. Diversity Characteristics

Envelope correlation coefficient (ECC), diversity gain (DG), multiplexing efficiency (ME), channel capacity loss (CCL), and total active reflection coefficient (TARC) are important parameters to characterize the diversity performance of MIMO antennas. ECC is mainly used to measure the correlation between MIMO antenna units. In order to obtain better diversity characteristics between MIMO antenna units, ECC should be as low as possible. Generally, the acceptable range of ECC shall be less than 0.5. For MIMO antennas, the envelope correlation coefficient can be calculated by the formula in [46]. The diversity gain and multiplexing efficiency can be calculated by formulas (7) and (8) [47].

$$DG = 10\sqrt{1 - ECC^2} \tag{7}$$

$$\eta_{mux} = \sqrt{\eta_i \eta_j (1 - |\rho_c|^2)} \tag{8}$$

Generally, the channel capacity of MIMO system changes linearly with the increase of the number of antenna units used. However, the correlation between antenna elements in MIMO channel system will cause capacity loss. Therefore, CCL is an important parameter to characterize the channel capacity of a MIMO system. Generally, the expected value of CCL is less than 0.4 bps/Hz. For two port MIMO antennas, the CCL can be calculated by the formula in [48]. TARC is defined as the square root of the ratio of total reflected power to total incident power. For MIMO systems, the expected value of TARC is less than 0 dB. For two port MIMO antennas, TARC can be calculated by formula (9).

$$\text{TARC} = \sqrt{\frac{(S_{11} + S_{12})^2 + (S_{21} + S_{22})^2}{2}} \tag{9}$$

The envelope correlation coefficient and diversity gain performance of the antenna are shown in Fig. 16, from which it can be observed that the ECC of the antenna is less than 0.01 in the whole UWB. The DG of the antenna is greater than 9.8 dB. In particular, ECC and DG have small fluctuations in the frequency bands of 6.2–7.8 GHz and 10.6–11.8 GHz, which is mainly caused by the non-resonant characteristics of the antenna in these two frequency bands.

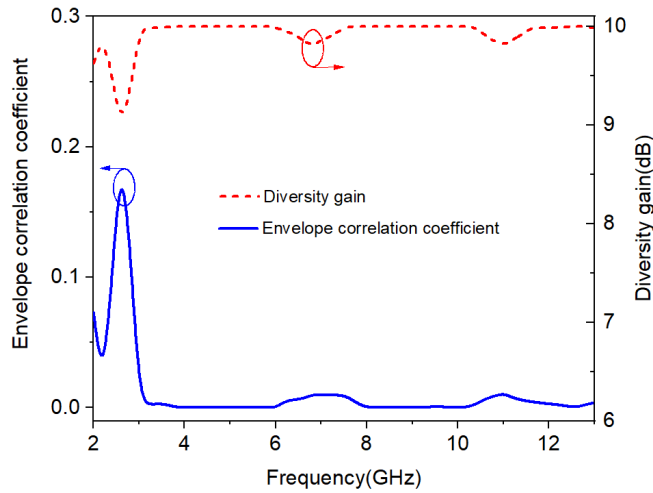


Figure 16. Envelope correlation coefficient and diversity gain of the proposed antenna.

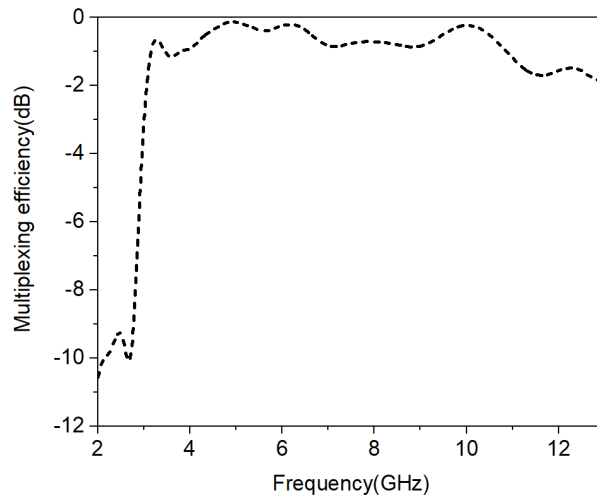


Figure 17. Multiplexing efficiency of the proposed antenna.

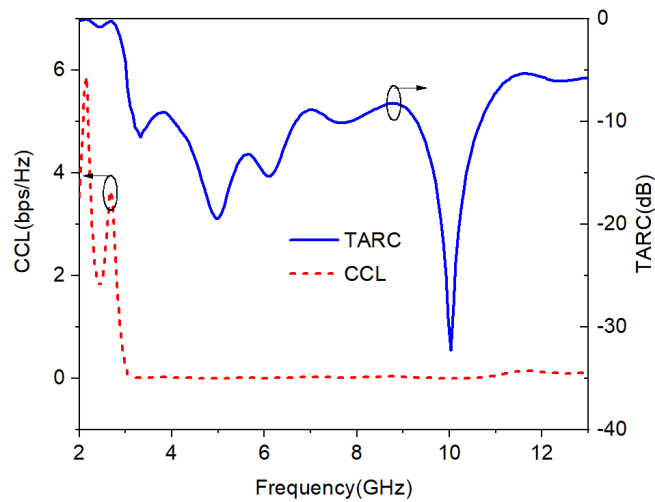


Figure 18. The CCL and TARC of the proposed antenna.

The multiplexing efficiency of the antenna is shown in Fig. 17. It can be seen that the multiplexing efficiency of the antenna is less than -1.0 dB in the 3.1–10.9 GHz band. In the 10.9–12.6 GHz frequency band, the multiplexing efficiency is less than -1.7 dB. The maximum multiplexing efficiency is -0.12 dB. Therefore, the antenna achieves high multiplexing efficiency in the whole impedance bandwidth, especially in the UWB.

The CCL and TARC characteristics of the antenna are shown in Fig. 18. It can be observed that in the whole impedance bandwidth, the CCL values are less than 0.08 bps/Hz and TARC values less than -4.1 dB. In UWB, CCL value is less than 0.03 bps/Hz and TARC value less than -8.5 dB.

Table 2. Performance comparison with some representative published literatures.

Ref.	Size (mm ²)	Electrical dimensions	Bandwidth (GHz)	Gain (dBi)	Isolation (dB)	ECC	Diversity Gain (dB)	Structure
[49]	24 × 30	0.6λ × 0.8λ	3–12.6	2–4.8	> 16.3	< 0.05	> 9.8	Fractal Monopole and DGS
[50]	23 × 40	0.5λ × 0.9λ	2–11	2.0–6.0	> 17	< 0.15	> 9.7	Monopole and DGS
[51]	50 × 40	1.2λ × 1.0λ	2.7–12.0	2.0–5.7	> 17	< 0.03	NA	Monopole and DGS
[52]	35 × 35	0.9λ × 0.9λ	3.0–12.0	3.0 stable	> 15	< 0.07	NA	Monopole and DGS
[53]	19 × 30	0.4λ × 0.7λ	3.1–10.6	1.2–2.91	> 18	< 0.03	> 9.7	Monopole and DGS
[35]	50 × 85	1.0λ × 1.7λ	2–9.5	1.5–4.0	> 20	< 0.03	NA	Partially shared
[31]	40 × 100	0.5λ × 1.2λ	GSM-LTE bands	NA	> 20	NA	NA	Radiator-ground shared
This work	48 × 58	1.1λ × 1.3λ	2.7–12.6 3.0–11.0	3.1–7.3	90% bandwidth > 20 10% bandwidth > 16	< 0.01	> 9.8	Radiator-ground shared

4.5. Performance Comparison

As mentioned above, there are some reports on UWB-MIMO ground antenna at present. In view of this, the performance comparison among the UWB-MIMO coplanar ground antenna designed in this paper and some representative published literatures in recent years is shown in Table 2, where λ is the wavelength corresponding to the center frequency of the antenna bandwidth. It is observed that the designed antenna has achieved a good trade-off in performance characteristics, such as geometric size, impedance bandwidth, gain, isolation, and diversity.

5. CONCLUSION

Based on the design method of UWB-MIMO antenna by using characteristic mode theory, multistage stepped and double L-shaped patches are introduced for designing the proposed antenna. By introducing capacitive and capacitive-inductive loading, multiple different characteristic modes combinations of metal ground in UWB are successfully excited at different ports of the antenna, so as to realize the bandwidth broadening, isolation improvement, and geometric size reduction of the coplanar ground antenna. The designed antenna structure is simple and compact, and there is no additional isolation and decoupling structure. The simulated and measured results show that the designed antenna achieves a good trade-off in geometric size, impedance bandwidth, isolation, and diversity. Therefore, the designed antenna can meet the practical application requirements of new mobile terminals or platforms in space constraints, broadband, and high data rate.

ACKNOWLEDGMENT

This work was supported by the National Natural Science Foundation of China (No. 61875054, No. 61905074), the Foundation of Science and Technology on Communication Networks Laboratory, China (No. 6142104190315), Hunan Provincial Natural Science Foundation of China (No. 2020JJ4318, No. 2019JJ50170, 2020JJ7007), and the Foundation of National key Laboratory for Complex Systems Simulation, China (No. XM2020XT 1004).

REFERENCES

1. Li, M. J. and N. Behdad, "A compact, capacitively fed UWB antenna with monopole-like radiation characteristics," *IEEE Trans. Antennas Propag.*, Vol. 65, 1026–1035, 2017.
2. Liu, J. L., J. P. Geng, and K. Wang, "A low-profile, directional, ultrawideband antenna," *IEEE Antennas Wireless Propag. Lett.*, Vol. 18, 255–259, 2019.
3. Tang, Z., X. F. Wu, and J. Zhan, "A novel miniaturized antenna with multiple band notched characteristics for UWB communication applications," *Journal of Electromagnetic Waves and Applications*, Vol. 32, 1961–1972, 2018.
4. Nie, L. Y., X. Q. Lin, and Z. Q. Yang, "Structure-shared planar UWB MIMO antenna with high isolation for mobile plat-form," *IEEE Trans. Antennas Propag.*, Vol. 67, 2735–2738, 2019.
5. Tang, Z. J., J. Zhan, and X. F. Wu, "Simple ultra-wider bandwidth MIMO antenna integrated by double decoupling branches and square-ring ground structure," *Microw. Opt. Technol. Lett.*, Vol. 62, 1259–1266, 2020.
6. Zhao, X. W., R. Sharjeel, and S. Y. Geng, "A reconfigurable MIMO/UWB MIMO antenna for cognitive radio applications," *IEEE Access*, Vol. 7, 46739–46747, 2019.
7. Liu, Y. Y. and Z. H. Tu, "Compact differential band-notched stepped-slot UWB-MIMO antenna with common-mode suppression," *IEEE Antennas Wireless Propag. Lett.*, Vol. 16, 593–595, 2017.
8. Yu, C. Y., S. H. Yang, and Y. C. Chen, "A super-wideband and high isolation MIMO antenna system using a wind-mill-shaped decoupling structure," *IEEE Access*, Vol. 8, 115767–115777, 2020.

9. Li, Y. S., W. X. Li, and Q. B. Ye, "A reconfigurable triple-notch-band antenna integrated with defected microstrip structure band-stop filter for ultra-wideband cognitive radio applications," *International Journal of Antennas and Propag.*, Vol. 7, 1–13, 2013.
10. Mao, C. X. and Q. X. Chu, "Compact coradiator UWB-MIMO antenna with dual polarization," *IEEE Trans. Antennas Propag.*, Vol. 62, 4474–4480, 2014.
11. Li, J. F., Q. X. Chu, and Z. H. Li, "Compact dual band-notched UWB MIMO antenna with high isolation," *IEEE Trans. Antennas Propag.*, Vol. 61, 4759–4766, 2013.
12. Zhang, J., L. Wang, and W. Zhang, "A novel dual band-notched CPW-fed UWB MIMO antenna with mutual coupling reduction characteristics," *Progress In Electromagnetics Research Letters*, Vol. 90, 21–28, 2020.
13. Tang, X., Z. Yao, and Y. Li, "A high performance UWB MIMO antenna with defected ground structure and U-shape branches," *International Journal of RF and Microwave Computer-Aided Engineering*, Vol. 31, 22270–22283, 2020.
14. Tang, Z. J., J. Zhan, and X. F. Wu, "Design of a compact UWB MIMO antenna with high isolation and dual band notched characteristics," *Journal of Electromagnetic Waves and Applications*, Vol. 34, 500–513, 2020.
15. Lin, G. S., C. H. Sung, and J. L. Chen, "Isolation improvement in UWB MIMO antenna system using carbon black film," *IEEE Antennas Wireless Propag. Lett.*, Vol. 16, 222–225, 2016.
16. Mathur, R. and S. Dwari, "Compact CPW-Fed ultra wideband MIMO antenna using hexagonal ring monopole antenna elements," *AEU-Int. J. Electron. Commun.*, Vol. 93, 1–6, 2018.
17. Wang, Y. H., Y. J. Yang, and Q. X. Chi, "Design of a compact ultra-wideband MIMO antenna," *The Journal of Engineering*, Vol. 20, 6487–6489, 2019.
18. Gunjan, S. and M. Akhilesh, "Compact MIMO slot antenna for UWB applications," *IEEE Antennas Wireless Propag. Lett.*, Vol. 15, 1057–1060, 2015.
19. Luo, C. M., J. S. Hong, and L. L. Zhong, "Isolation enhancement of a very compact UWB-MIMO slot antenna with two defected ground structures," *IEEE Antennas Wireless Propag. Lett.*, Vol. 14, 1766–1769, 2015.
20. Rohit, G., K. U. Dharmendra, and K. Binodk, "A novel compact self-similar fractal UWB MIMO antenna," *International Journal of RF and Microwave Computer-Aided Engineering*, Vol. 29, 21632–21641, 2019.
21. Muhammad, S. K., A. D. Capobianco, and I. Adnan, "Ultra-compact dual-polarised UWB MIMO antenna with meandered feeding lines," *IET Microwaves, Antennas & Propag.*, Vol. 11, 997–1002, 2017.
22. Wang, L. L., Z. H. Du, and H. L. Yang, "Compact UWB MIMO antenna with high isolation using fence-type decoupling structure," *IEEE Antennas Wireless Propag. Lett.*, Vol. 18, 1641–1645, 2019.
23. Rakesh, N. T., S. Prabhakar, and K. K. Binod, "Neutralization technique based two and four port high isolation MIMO antennas for UWB communication," *AEU-Int. J. Electron. Commun.*, Vol. 110, 152828–152850, 2019.
24. Vutukuyi, S., O. P. Pokkunuri, and T. P. M. Boddapati, "Dual band notched orthogonal 4-element MIMO antenna with isolation for UWB applications," *IEEE Access*, Vol. 8, 145871–145880, 2020.
25. Syedakbar, S., S. Ramesh, and J. Deepa, "Ultra wideband monopole planar MIMO antenna for portable devices," *IEEE International Conference on Electrical, Instrumentation and Communication Engineering (ICEICE)*, 1–4, Karur, India, 2017.
26. Hasan, M. N., S. Chu, and S. Bashir, "A DGS monopole antenna loaded with U-shape stub for UWB MIMO applications," *Microw. Opt. Technol. Lett.*, Vol. 61, 2141–2149, 2019.
27. Li, Q., A. P. Feresidis, and M. Mavidou, "Miniaturized double-layer EBG structures for broadband mutual coupling reduction between UWB monopoles," *IEEE Trans. Antennas Propag.*, Vol. 63, 1168–1171, 2015.
28. Roshna, T. K., K. U. Deepa, and P. Mohanaan, "Compact UWB MIMO antenna for tridirectional pattern diversity characteristics," *IET Microwaves, Antennas & Propag.*, Vol. 11, 2059–2065, 2017.

29. Guo, J. Y., F. Liu, and L. Y. Zhao, "Meta-surface antenna array decoupling designs for two linearly polarized antennas coupled in H -plane and E -plane," *IEEE Access*, Vol. 7, 100442–100452, 2019.
30. Luo, S. Y., Y. S. Li, and Y. F. Xia, "A low mutual coupling antenna array with gain enhancement using metamaterial loading and neutralization line structure," *Applied Computational Electromagnetics Society Journal*, Vol. 34, 411–418, 2019.
31. Li, H., B. K. Lau, and Z. Ying, "Decoupling of multiple antennas in terminals with chassis excitation using polarization diversity, angle diversity and current control," *IEEE Trans. Antennas Propag.*, Vol. 60, 5947–5957, 2012.
32. Ghalib, A. and M. S. Sharawi, "TCM analysis of defected ground structures for MIMO antenna designs in mobile terminals," *IEEE Access*, Vol. 5, 19680–19692, 2017.
33. Manteuffe, D. and R. Martens, "Compact multimode multielement antenna for indoor UWB massive MIMO," *IEEE Trans. Antennas Propag.*, Vol. 64, 2689–2697, 2016.
34. Erik, F. A., P. M. Angel, and G. V. Ricardo, "Characteristic mode analysis applied to reduce the mutual coupling of a four-element patch MIMO antenna using a defected ground structure," *IET Microwaves, Antennas & Propag.*, Vol. 14, 215–226, 2020.
35. Zhao, X., S. P. Yeo, and L. C. Ong, "Planar UWB MIMO antenna with pattern diversity and isolation improvement for mobile platform based on the theory of characteristic modes," *IEEE Trans. Antennas Propag.*, Vol. 66, 420–425, 2018.
36. Tang, Z.-J., L. Liang, B. Zhong, L. Cheng, C. Tan, and S. Hu, "Uniplanar UWB-MIMO antenna with high isolation based on the radiator-ground shared structure," *Progress In Electromagnetics Research Letters*, Vol. 93, 35–42, 2020.
37. Li, K. and Y. Shi, "A pattern reconfigurable MIMO antenna design using characteristic modes," *IEEE Access*, Vol. 6, 43526–43534, 2018.
38. Liang, Z. P., J. Ouyang, and F. Yang, "Design and characteristic mode analysis of a low-profile wideband patch antenna using metasurface," *Journal of Electromagnetic Waves and Applications*, Vol. 32, 2304–2313, 2018.
39. Martens, R., E. Safin, and D. Manteuffel, "Inductive and capacitive excitation of the characteristic modes of small terminals," *IEEE Loughborough Antennas & Propagation Conference*, 1–4, Loughborough, UK, 2011.
40. Li, K. and Y. Shi, "A pattern reconfigurable MIMO antenna design using characteristic modes," *IEEE Access*, Vol. 6, 43526–43534, 2018.
41. Martens, R. and D. Manteuffel, "Systematic design method of a mobile multiple antenna system using the theory of characteristic modes," *IET Microwaves, Antennas & Propag.*, Vol. 8, 887–893, 2014.
42. Wang, C. H., Y. K. Chen, and S. W. Yang, "Application of characteristic mode theory in HF band aircraft-integrated multi-antenna system designs," *IEEE Trans. Antennas Propag.*, Vol. 67, 513–521, 2019.
43. Kim, D. Woo, and S. Nam, "Systematic design of a multiport MIMO antenna with bilateral symmetry based on characteristic mode analysis," *IEEE Trans. Antennas Propag.*, Vol. 66, 1076–1085, 2018.
44. Shih, T. Y. and N. Behdad, "Bandwidth enhancement of platform-mounted HF antennas using the characteristic mode theory," *IEEE International Symposium on Antennas and Propagation & USNC/URSI National Radio Science Meeting*, 1–12, Vancouver, BC, Canada, 2015.
45. Kishor, K. K. and S. V. Hum, "Multi-port multi-band chassis-mode antenna design using characteristic modes," *IEEE Antennas Wireless Propag. Lett.*, Vol. 16, 609–612, 2016.
46. Tang, Z., X. F. Wu, and J. Zhan, "Compact UWB-MIMO antenna with high isolation and triple band-notched characteristics," *IEEE Access*, Vol. 7, 19856–19865, 2019.
47. Khan, M. S., A. D. Capobianco, and S. M. Asif, "A compact CSRR enabled UWB diversity antenna," *IEEE Antennas Wireless Propag. Lett.*, Vol. 16, 808–812, 2016.

48. Ali, W. and A. Ibrahim, "A compact double-sided MIMO antenna with an improved isolation for UWB applications," *AEU-Int. J. Electron. Commun.*, Vol. 82, 7–13, 2017.
49. Gurjar, R., D. K. Upadhyay, B. K. Kanaujia, and A. Kumar, "A compact modified sierpinski carpet fractal UWB MIMO antenna with square-shaped funnel-like ground stub," *AEU-Int. J. Electron. Commun.*, Vol. 117, 1–10, 2020.
50. Thakur, E., N. Jaglan, S. D. Gupta, and B. Kanaujia, "A compact notched UWB MIMO antenna with enhanced performance," *Progress In Electromagnetics Research C*, Vol. 91, 39–53, 2019.
51. Khan, S. M., A. Iftikhar, S. M. Asif, A. D. Capobianco, and B. D. Braaten, "A compact four elements UWB MIMO antenna with on-demand WLAN rejection," *Microw. Opt. Technol. Lett.*, Vol. 58, No. 2, 270–276, 2016.
52. Wani, Z. and D. Kumar, "A compact 4×4 MIMO antenna for UWB applications," *Microw. Opt. Technol. Lett.*, Vol. 58, 1433–1436, 2016.
53. Kumar, A., A. Q. Ansari, B. K. Kanaujia, J. Kishor, and S. Kumar, "An ultra-compact two-port UWB-MIMO antenna with dual band-notched characteristics," *AEU-Int. J. Electron. Commun.*, Vol. 114, 1–12, 2020.